JOURNAL OF PROPULSION AND POWER
Vol. 13, No. 6, November–December 1997

Zonal Approach for Prediction of Jet Noise

S. H. Shih,* D. R. Hixon,* and R. R. Mankbadi†
NASA Lewis Research Center, Cleveland, Ohio 44135

A zonal approach for direct computation of sound generation and propagation from a supersonic jet is investigated. The present work splits the computational domain into a nonlinear, acoustic-source regime and a linear acoustic wave propagation regime. In the nonlinear regime, the unsteady flow is governed by the large-scale equations, which are the filtered compressible Navier–Stokes equations. In the linear acoustic regime, the sound wave propagation is described by the linearized Euler equations. Computational results are presented for a supersonic jet at $M = 2.1$. It is demonstrated that no spurious modes are generated in the matching region and the computational expense is reduced as opposed to fully large-scale simulation.

Nomenclature

C_s = Smagorinsky's constant
c_v = specific heat for constant volume
E = total energy
$\boldsymbol{F}$ = flux vector in axial direction
$\bar{\boldsymbol{F}}$ = disturbance flux vector in axial direction
$\boldsymbol{G}$ = flux vector in radial direction
$\bar{\boldsymbol{G}}$ = disturbance flux vector in radial direction
I = total enthalpy
k = thermal conductivity
p = static pressure
$\boldsymbol{Q}$ = dependent variables vector for the resolved (filtered) field
$\bar{\boldsymbol{Q}}$ = dependent variables vector for the disturbance field
q = fine-scale turbulence heat conduction
R, D = nozzle radius, diameter
S = source term
$\bar{S}$ = source term for the linearized Euler equations
$\bar{S}_{ij}$ = strain rate of the resolved field
T = static temperature
U_e = jet exit centerline velocity
U, V = mean flow velocities in axial and radial directions
u, v = velocity components in axial and radial directions
Δ_f = filter width
Δ_x, Δ_r = grid spacings in axial and radial directions
ν_R = effective viscosity of the residual field
ρ = density
σ_{ij} = viscous stresses
τ_{ij} = unresolved stresses

Introduction

In theory, direct numerical simulation (DNS) based on the compressible Navier–Stokes equations provides both the flow fluctuations and the acoustic field. However, the resolution requirement for high Reynolds number turbulent flows makes direct numerical simulation impractical because of current computer limitations. It is known that the large-scale structure is responsible for the generation of the dominant part of supersonic jet noise.[1–6] This indicates that it is appropriate to perform large-eddy simulations (LES) to accurately capture the large scales of motion while modeling the subgrid scale turbulence. The large-scale structure can be described by the nonlinear instability theory. According to the stochastic instability wave model,[7,8] the large-scale structures and instability waves of the jet are statistically equivalent. The fine-scale turbulence (which is the unresolved scale), contributes to noise in two ways: 1) directly, but it is not accounted for in LES, and 2) indirectly, as it alters the mean flow (jet axial core, shear-layer thickness) and the large-scale structure. This is accounted for in LES through the use of the subgrid scale model.

The use of LES as a tool for the prediction of the jet noise source has been proposed by Mankbadi et al.,[9] in which the computed fluctuating sound source in the near field was then used to obtain the far-field sound through the application of Lighthill's theory. Because of the noncompactness of the source and the need to account for the retarded time, accurate application of Lighthill's theory requires prohibitive computer storage. Later, Mankbadi et al.[10] extended the computational domain to the acoustic field, where large-scale equations are solved for both the sound source and the acoustic fields for the axisymmetric case. The approach was extended in Shih et al.,[11] to the three-dimensional case, but was restricted to the near region because of computer limitations. An alternative approach for extending the three-dimensional computation to the far field is needed.

Hardin and Pope[12,13] proposed a two-part calculation where the viscous flow was first handled by calculating the time-dependent incompressible flow, and then the acoustic radiation was obtained from inviscid equations describing the differences from the incompressible flow. The time-dependent incompressible viscous flow was calculated first; the acoustic field can be obtained through integration of the disturbances equations that contain the time-dependent incompressible solution as coefficients and forcing terms. Viswanathan and Sankar[14] developed a numerical technique for the direct calculation of flow-generated noise and applied it to the prediction of supersonic jet noise. In their approach, each flow parameter is decomposed into a time-averaged mean and a time-dependent fluctuating part. The mean flow is established with the solution of the Reynolds-averaged compressible Navier–Stokes equations in the first step. The flow perturbations based on the description of the large-scale structures as a linear superposition of normal mode instability waves are obtained through solution of the linearized Euler equations for the fluctuation variables. Good comparisons of the radiated noise with experiments were obtained. The use of linearized Euler equations for the prediction of supersonic jet noise, similar to the ap-

Presented as Paper 95-144 at the AIAA/CEAS 1st Joint Aeroacoustics Conference, Munich, Germany, June 12–15, 1995; received Feb. 5, 1997; revision received May 27, 1997; accepted for publication June 6, 1997.

*Senior Research Associate, Institute for Computational Mechanics in Propulsion, Ohio Aerospace Institute, M/S 5-11. Member AIAA.

†Senior Scientist, Institute for Computational Mechanics in Propulsion, Ohio Aerospace Institute; currently, Professor at Cairo University, Cairo, Egypt. Associate Fellow AIAA.

proach by Viswanathan and Sankar,[14] was also reported by Mankbadi et al.,[15] where the mean flow solution was extracted from the experimental measurements.

An acoustic calculation can be viewed as consisting of two parts, one describing the nonlinear generation of sound, the other describing the linear propagation of sound. All nonlinear flow effects and source generation are confined to the near field and can be computed by large-scale equations. There are several approaches to calculate the sound propagation once the source has been identified, such as acoustic analogy, Kirchhoff's method,[16] and linearized Euler equations. Freund et al.[17] studied the matching of near/far-field equation sets for computations of aerodynamic sound. Their results of an acoustic source embedded in a shear layer using linearized Euler equations as the far-field equation set are encouraging.

In the present work, the near-field source region solution including all nonlinear flow hydrodynamics is obtained through the large-scale equations[10] and is matched to the solution of the linearized Euler equations governing the acoustic field. The present research combines the large-scale simulation and linearized Euler equations approach into one computer code, resulting in the saving of computer CPU time for extension to three-dimensional acoustic field predictions.

Governing Equations

The computational domain (Fig. 1) is split into nonlinear source generation and linear acoustic propagation regions, which are governed by the large-scale and linearized Euler equations, respectively.

Large-Scale Equations

The flowfield of a supersonic jet is governed by the compressible Navier–Stokes equations and can be decomposed into filtered and residual fields, namely,

$$f = \bar{f} + f'' \tag{1}$$

where an overbar denotes the resolved (filtered) field, and a double-prime denotes the unresolved (subgrid) field.[18] The mean of the filtered field is the mean of the total field. Upon substituting this splitting in the full Navier–Stokes equations, the filtered compressible Navier–Stokes equations in cylindrical coordinates take the form

$$\frac{\partial \boldsymbol{Q}}{\partial t} + \frac{\partial \boldsymbol{F}}{\partial x} + \frac{1}{r}\frac{\partial}{\partial r}(r\boldsymbol{G}) = S \tag{2}$$

where

$$\boldsymbol{Q} = (\bar{\rho}, \bar{\rho}\tilde{u}, \bar{\rho}\tilde{v}, \bar{\rho}\tilde{E})^T \tag{3}$$

$$\boldsymbol{F} = \begin{bmatrix} \bar{\rho}\tilde{u} \\ \bar{p} + \bar{\rho}\tilde{u}^2 - \tilde{\sigma}_{xx} - \tau_{xx} \\ \bar{\rho}\tilde{u}\tilde{v} - \tilde{\sigma}_{xr} - \tau_{xr} \\ \bar{\rho}\tilde{u}\tilde{I} - \tilde{u}\tilde{\sigma}_{xx} - \tilde{v}\tilde{\sigma}_{xr} - k\dfrac{\partial}{\partial x}\tilde{T} - c_v q \end{bmatrix} \tag{4}$$

$$\boldsymbol{G} = \begin{bmatrix} \bar{\rho}\tilde{v} \\ \bar{\rho}\tilde{u}\tilde{v} - \tilde{\sigma}_{xr} - \tau_{xr} \\ \bar{p} + \bar{\rho}\tilde{v}^2 - \tilde{\sigma}_{rr} - \tau_{rr} \\ \bar{\rho}\tilde{v}\tilde{I} - \tilde{u}\tilde{\sigma}_{xr} - \tilde{v}\tilde{\sigma}_{rr} - k\dfrac{\partial}{\partial r}\tilde{T} - c_v q \end{bmatrix} \tag{5}$$

$$S = \frac{1}{r}\begin{bmatrix} 0 \\ 0 \\ \bar{p} - \tilde{\sigma}_{\phi\phi} - \tau_{\phi\phi} \\ 0 \end{bmatrix} \tag{6}$$

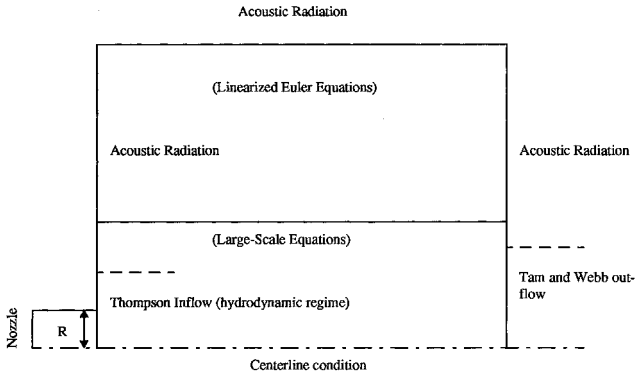

Fig. 1 Computational domain.

Here $\boldsymbol{Q}$ is the unknown vector, $\boldsymbol{F}$ and $\boldsymbol{G}$ are the fluxes in the x and r directions, respectively, and S is the source term that arises in cylindrical polar coordinates. This system of equations is coupled with the equation of state for a perfect gas. Here, a tilde denotes Favre filtering:

$$\tilde{f} = \overline{\rho f}/\bar{\rho} \tag{7}$$

The unresolved stresses τ_{ij} appearing in Eqs. (4–6) need to be modeled.

Linearized Euler Equations

Starting from the full Navier–Stokes equations in conservation form, neglecting viscosity, and linearizing about a mean flow (U, V), the axisymmetric linearized Euler equations may be written in cylindrical coordinates as

$$\frac{\partial \bar{\boldsymbol{Q}}}{\partial t} + \frac{\partial \bar{\boldsymbol{F}}}{\partial x} + \frac{1}{r}\frac{\partial}{\partial r}(r\bar{\boldsymbol{G}}) = \bar{S} \tag{8}$$

where

$$\bar{Q} = (\hat{\rho}, \hat{u}, \hat{v}, \hat{e}) = [\rho', (\rho u)', (\rho v)', (\rho e)'] \tag{9}$$

$$\boldsymbol{F} = \begin{bmatrix} \hat{u} \\ p' + 2\hat{u}U - \hat{\rho}U^2 \\ \hat{u}V + \hat{v}U - \hat{\rho}UV \\ (p' + \hat{e})U + (\hat{u} - \hat{\rho}U)E \end{bmatrix} \tag{10}$$

$$\bar{\boldsymbol{G}} = \begin{bmatrix} \hat{v} \\ \hat{u}V + \hat{v}U - \hat{\rho}UV \\ p' + 2\hat{v}V - \hat{\rho}V^2 \\ (p' + \hat{e})V + (\hat{v} - \hat{\rho}V)E \end{bmatrix} \tag{11}$$

$$\bar{S} = \begin{bmatrix} 0 \\ 0 \\ p'/r \\ 0 \end{bmatrix} \tag{12}$$

$$p' = (\gamma - 1)[\hat{e} - (\hat{u}U + \hat{v}V) + \tfrac{1}{2}\hat{\rho}(U^2 + V^2)] \tag{13}$$

In this notation the prime represents the disturbance field. The velocities are normalized by U_e, time by R/U_e, density by the mean exit centerline value, and pressure by the exit dynamic pressure.

Subgrid-Scale Modeling

The effect of unresolved scales on resolved ones is accounted for through the use of Smagorinsky's subgrid-scale model.[19] The subgrid-scale turbulence stresses are represented as follows:

$$\tau_{ij} = -k_g(\delta_{ij}/3) + 2\rho\nu_R(\tilde{S}_{ij} - \tfrac{1}{3}\delta_{ij}\tilde{S}_{mm}) \tag{14}$$

where k_g is the kinetic energy of the residual turbulence and is neglected with respect to the thermodynamic pressure. The strain rate of the resolved scale is given by

$$\tilde{S}_{ij} = \frac{1}{2}\left(\frac{\partial \tilde{u}_i}{\partial x_j} + \frac{\partial \tilde{u}_j}{\partial x_i}\right) \tag{15}$$

The summation S_{mn} is zero for incompressible flow, ν_R is

$$\nu_R = (C_s\Delta_f)^2 \cdot \sqrt{2S_{mn}S_{mn}} \tag{16}$$

and Δ_f is given by

$$\Delta_f = (\Delta_x\Delta_r)^{1/2} \tag{17}$$

For the heat equation, Edison[20] proposed the eddy viscosity model

$$q = \bar{\rho}\frac{\nu_R}{Pr_t}\frac{\partial \tilde{T}}{\partial x_k} \tag{18}$$

where Pr_t is the subgrid-scale turbulent Prandtl number, which can be taken as 0.5. Smagorinsky's constant C_s in Eq. (16) is 0.1, as used in the previous study.[10]

Numerical Method

The importance of the dispersion and dissipation of a given scheme, used in connection with the computational aeroacoustics, was highlighted by Hardin.[21] Both effects are crucial in computational aeroacoustics and can render the computed unsteady part of the solution completely unacceptable. As such, higher-order accurate schemes are required for problems in computational aeroacoustics.

A fourth-order accurate in space, second-order accurate in time scheme is used, which is an extension of the MacCormack scheme by Gottlieb and Turkel.[22] This scheme has been used extensively by other researchers.[23–28] In this scheme, the operator is split into two one-dimensional operators and applied in a symmetric way to avoid biasing of the solution. For the axisymmetric case, it can be written as

$$\boldsymbol{Q}^{n+2} = L_xL_rL_rL_x\boldsymbol{Q}^n \tag{19}$$

Each L operator consists of a predictor and corrector steps; each step uses a one-sided difference. For the streamwise direction, it takes the following form.

Predictor:

$$\boldsymbol{Q}_i^{n+1/2} = \boldsymbol{Q}_i^n - \frac{\Delta t}{6\Delta x}(7\boldsymbol{F}_i - 8\boldsymbol{F}_{i-1} + \boldsymbol{F}_{i-2})^n \tag{20}$$

Corrector:

$$\boldsymbol{Q}_i^{n+1} = \frac{1}{2}\left[\boldsymbol{Q}_i^n + \boldsymbol{Q}_i^{n+1/2} + \frac{\Delta t}{6\Delta x}(7\boldsymbol{F}_i - 8\boldsymbol{F}_{i+1} + \boldsymbol{F}_{i+2})^{n+1/2}\right] \tag{21}$$

and likewise for the other directions. At the computational boundaries, the flux quantities outside the boundaries are needed to perform the spatial derivatives, and these can be obtained using third-order extrapolation based on data from the interior of the domain.

Boundary Conditions

The boundary condition is an important issue in the computation of jet noise. Proper boundary treatment should allow waves to pass through the boundary without generating reflecting waves. Several boundary treatments were considered,[29] and it was shown that the boundary treatments used in Ref. 10 were stable, nonreflecting, and the most suitable for jet computations. The present work employs the same boundary treatments as in Ref. 10. The schematic diagram of Fig. 1 shows various boundary conditions used at each boundary.

In the nonlinear acoustic source region, the inflow boundary is split into fluid disturbance and acoustic radiation regimes. The inflow disturbances at the nozzle exit are both turbulent fluid disturbances and acoustics. The acoustic ones come from the internally generated sound sources as well as from a feedback of the jet plume noise. The generated jet plume noise is associated with the unsteady structure of the jet plume, which must be associated with a disturbance (fluid or acoustic at the beginning of the jet). Because of the nature of the engine flow, the turbulent fluid disturbances are dominant over the engine–acoustic sources. As such, the small inflow disturbances are taken to be representing turbulent flow disturbances and are specified from the centerline to $r/D = 2$. The disturbance is assumed in the following form:

$$(u' \;\; v' \;\; p' \;\; \rho') = \mathcal{R}[\Phi(r)e^{i(\alpha x - \omega t)}] \tag{22}$$

The Orr-Sommerfeld equations are solved to obtain the complex wave number α as the eigenvalue corresponding to the frequency ω and the radial functions $\Phi(r)$ as the corresponding eigenfunctions:

$$\Phi(r) = [\hat{u}(r),\ \hat{v}(r),\ \hat{p}(r),\ \hat{\rho}(r)] \tag{23}$$

To obtain the disturbance solution, a mean flow must be specified at the inflow boundary. In the present work, the analytical functions proposed by Tam and Burton,[30] to fit the experimental data of Troutt and McLaughlin,[31] were used. The mean axial velocity is given by

$$U = \begin{cases} U_1 & \text{for} \quad r < h \\ \exp\left\{-\ell n(2)\left[\dfrac{r - h(x)}{b(x)}\right]^2\right\} & \text{for} \quad r > h \end{cases} \tag{24}$$

where $b(x)$ is the half-width of the annular mixing layer and is fitted to the experimental data. The radius of the potential core $h(x)$ is related to $b(x)$ through the conservation of momentum.[30]

For the supersonic regime, all characteristics travel in the flow direction. Thus, the primitive variables are given at $x = 0$, as outlined in the preceding text. In the subsonic regime, the following three characteristics are specified according to the linear stability solution:

$$\begin{aligned} p_t + \rho c u_t &= C_1 \\ p_t - c^2\rho &= C_2 \\ \rho c v_t &= C_3 \end{aligned} \tag{25}$$

The fourth characteristic is outgoing and is obtained from the interior solution:

$$p_t - \rho c u_t = C_4 \tag{26}$$

The four characteristic equations are then solved together to obtain the time derivatives of the variables, which are used to update the solution at the inflow boundary.

In the radiation regime ($r/D > 2$), the conventional acoustic radiation condition applies:

$$\boldsymbol{Q}_t = -\Gamma(\theta)\left(\frac{x}{\bar{R}}\boldsymbol{Q}_x + \frac{r}{\bar{R}}\boldsymbol{Q}_r + \frac{\boldsymbol{Q}}{\bar{R}}\right) \tag{27}$$

where

$$\boldsymbol{Q} = (u, v, p, \rho) \qquad \bar{R} = \sqrt{x^2 + r^2}$$
$$\Gamma(\theta) = c\left[\frac{x}{\bar{R}}M + \sqrt{1 - \left(\frac{r}{\bar{R}}M\right)^2}\right] \tag{28}$$

and M is the local Mach number and c is the sonic velocity. The spatial derivatives that appear in Eq. (27) are evaluated in an identical manner as the inner flow derivatives.

The outflow treatment is based on the asymptotic analysis of the linearized equations, as given by Tam and Webb.[32] The pressure condition is the same as that obtained by Bayliss and Turkel,[33] Enquist and Majda,[34] and Hagstrom and Hariharan,[35] namely,

$$p_t = -\Gamma(\theta)\left(\frac{x}{\bar{R}}p_x + \frac{r}{\bar{R}}p_r + \frac{p}{\bar{R}}\right) \tag{29}$$

However, for updating the rest of the primitive variables, Tam and Webb[32] have shown that the momentum and continuity equations should be used to account for the presence of entropy and vorticity waves at the outflow boundary. For the outflow regime of large radius with the local Mach number less than 0.01, the outflow condition is replaced by the conventional acoustic radiation condition [Eq. (27)].

The results presented herein are for an axisymmetric disturbance, for which the boundary condition at $r = 0$ can be stated as

$$\frac{\partial}{\partial r}(u, p, \rho) = 0; \quad v = 0 \tag{30}$$

The centerline treatment for nonaxisymmetric disturbances is not obvious, and was addressed by Shih et al.[11]

In the linear acoustic region, the radiation boundary condition of Eq. (27) is used because only the acoustic wave is of significance in this region.

Matching

In the present work, this scheme is applied to both the large-scale and linearized Euler equations. A schematic diagram of the computational domain is presented in Fig. 1. No boundary condition is needed in the matching region. The scheme requires fluxes at two grid points outside of the domain to update variables at the boundary. An overlapping region, consisting of four grid points in the radial direction, is made to allow variables at interior points to be passed between two domains. The variables of the two solution domains are the filtered quantities and the fluctuation quantities. The mean of the filtered field is the mean of the total field. Therefore, it is straightforward to set up a matching scheme at the interface. At every time step, all linear acoustic region variables in the overlap region are converted to nonlinear region variables and used to evaluate the fluxes in the nonlinear region. Likewise, at every time step, all nonlinear region variables are converted to linear acoustic region variables and they are used to evaluate the fluxes in the acoustic region. Freund et al.[17] pointed out that grid stretching and interpolation induce error in the calculation, though reducing the computing expense. The present simulation uses identical uniform grids in the overlapping region to avoid such generation of spurious waves.

Results and Discussion

The numerical simulation was conducted for a cold, nearly perfectly expanded axisymmetric supersonic jet of Mach number 2.1. The test case has been simulated previously[10] using large-scale equations. The total temperature of the jet is 294 K, and the jet exit pressure is 0.0515 atm. The Reynolds number based on exit conditions is approximately 7×10^4. In the present calculation, the jet is excited at a Strouhal number of 0.2 with the Strouhal number defined as $St = fD/U_e$, where D is the nozzle exit diameter.

The computational domain for this problem extends axially from $x/D = 2.5$ to 35, and radially from the centerline to $r/D = 16$, as shown in Fig. 1. Because of the steep mean flow gradient encountered at the jet exit, the computational grid was begun at an axial distance $x/D = 2.5$ from the actual jet exit. The computational grid consists of 391 equally spaced points in the axial direction. In the radial direction, 150 points are used and stretched between the centerline and $r/D = 2.5$, with a concentration of grid points around $r/D = 0.5$. Between $r/D = 2.5$–16, 130 equally spaced points are used, with a spacing equal to that of the last stretched points. The present computation uses 50 points per wavelength based on the inflow forcing frequency at a Strouhal number of 0.2. Because of the sharp flow gradient in the shear layer at nozzle exit, 60 grid points are placed inside the shear layer to account for the effect of fine-scale turbulence, which, for the present subgrid scale model used, is a function of grid sizes. The interface between the nonlinear and linear acoustic regions was chosen at $r/D = 5$, above which the mean flow is uniform throughout the domain.

Figure 2 shows the instantaneous distribution of ρ, p, u, and v at $t = 150$, where t is the characteristic time defined as the ratio of nozzle exit radius to the jet exit centerline velocity. The horizontal line at $r/D = 5$ in Fig. 2 indicates the boundary between the two domains. One can see smooth solutions across the matching region, although some kinks are observed in the axial velocity distribution. The disturbances generated in the shear layer propagate through the matching region to the far field without any distortion. The wave-like nature of the flowfield is evident and the solution is clean from boundary reflections.

Figure 3 shows contours of the rms values of the normalized pressure and axial momentum distributions. The contour levels are 0.00035 and 0.0025 for the rms values of pressure and axial momentum, respectively. No spurious disturbances are generated in the matching region, and the preferred forward emission is clearly shown in Fig. 3.

Figure 4 shows the axial development of the axial momentum fluctuations on the nozzle lip line. The computed results obtained using the large-scale equations throughout the computational domain[10] are also shown in Fig. 4. The present zonal approach gives the development of axial momentum fluctuations identical to those obtained in Ref. 10. Figure 5 shows the axial development of the rms values of the pressure on the nozzle lip line. Again, the result of zonal approach is identical to those in Ref. 10. The computational domain and grid size used for the present zonal approach are the same as the previous large-scale computation in Ref. 10.

Figure 6 compares the amplitude of pressure disturbance at $r/D = 12$ along the axial direction at $St = 0.2$, with the results from Ref. 10. Because of the use of linearized Euler equations in this region (no viscous dissipation), a slightly higher peak was obtained by the present approach. The overall distribution is consistent with the previous large-scale computed results.

Figure 7 presents the pressure spectra at $x/D = 25$, $r/D = 12$ for both zonal and large-scale approaches. The amplitude at fundamental frequency, $St = 0.2$, is slightly higher for the zonal approach, whereas it becomes lower at successive harmonics than the large-scale simulation results. Previous linearized Euler computation alone[15] did not show any generation of successive harmonics, except for the fundamental one.

Figure 8 shows the sound pressure level distribution in the far field for the present and previous calculations. The measured experimental data are also shown in Fig. 8. The calculated sound pressure level was scaled to match the maximum sound pressure level of 148 dB at $r/D = 10$ in the experiment. The procedure is necessary because one does not know the

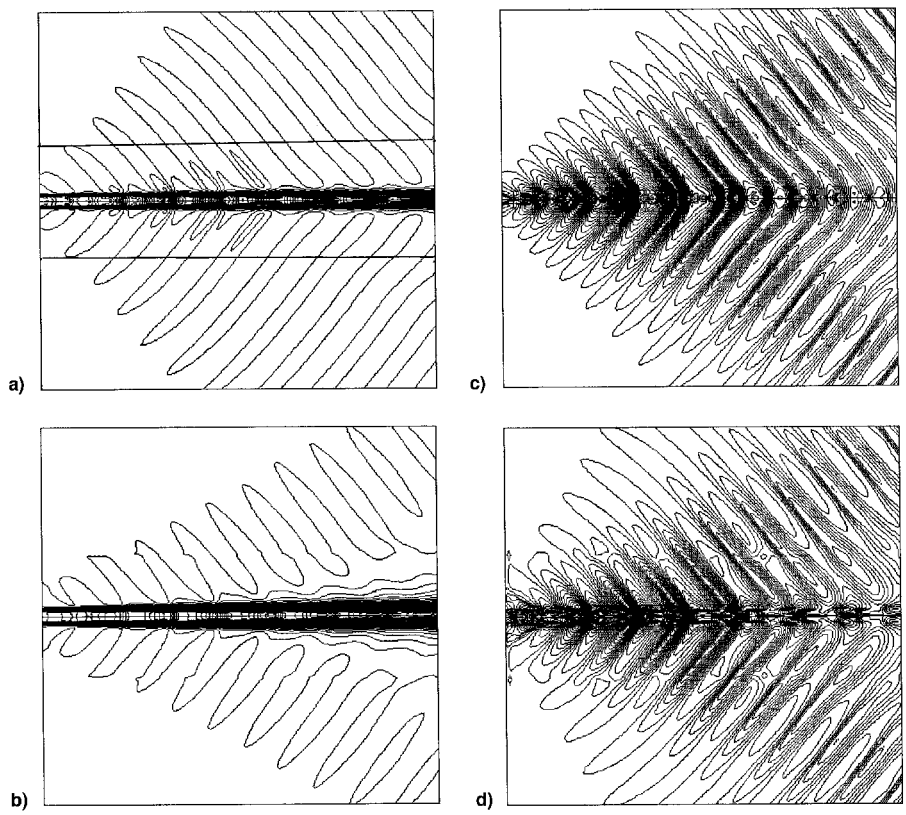

Fig. 2 Instantaneous distribution of a) density at $t = 150$, $r_{max} = 1.1$, $r_{min} = 0.45$, 41 contours; b) axial velocity at $t = 150$, $u_{max} = 1.1$, $u_{min} = -0.1$, 41 contours; c) pressure at $t = 150$, $p_{max} = 0.178$, $p_{min} = 0.14$, 41 contours; and d) radial velocity at $t = 150$, $v_{max} = 0.046$, $v_{min} = -0.034$, 41 contours.

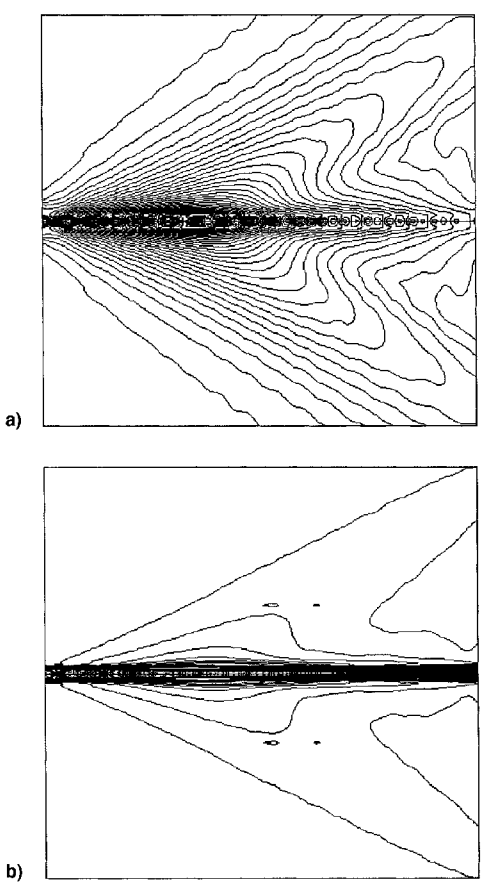

Fig. 3 Contours of rms values of a) pressure, maximum = 0.014, minimum = 0, 41 contours; and b) axial momentum, maximum = 0.1, minimum = 0.41 contours.

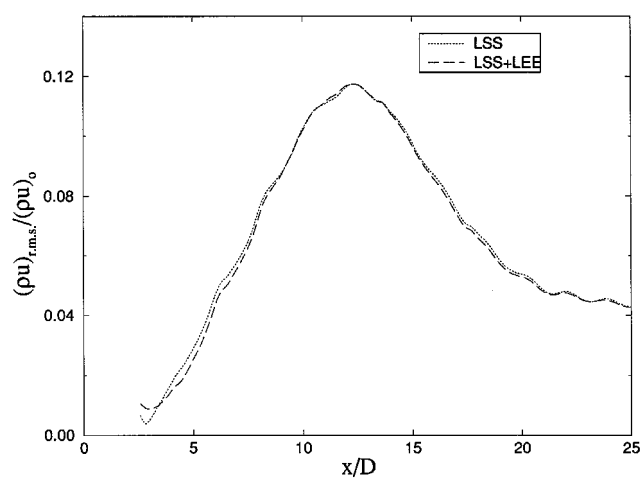

Fig. 4 Streamwise development of rms values of axial momentum in the shear layer, $r/D = 0.5$.

amplitude of disturbance at the nozzle exit. It is seen that the computed patterns of the sound pressure level contours are consistent with the previous work.[10] As pointed out in Ref. 10, the computed results show a downstream shift of the lobes when compared to the experimental measurements. This can be explained by the fact that the calculations are for an axisymmetric case, while the measurements showed that excited motion of the jet is dominated by the first helical mode in addition to the axisymmetric mode.[31]

Figure 9 shows the calculated and measured sound field directivity at a circle of radius $24D$, with the center at the jet exit centerline. The angle is measured from the jet exit centerline. The calculated peak occurs around 15 deg, which is the same as the one predicted in Ref. 10. The peak in the

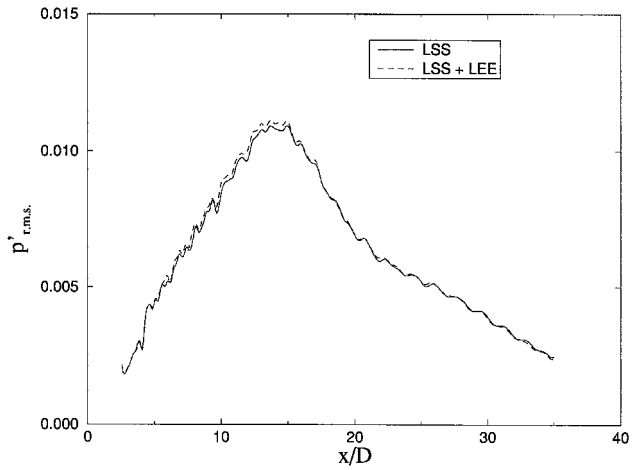

Fig. 5 Streamwise development of rms values of pressure in the shear layer, $r/D = 0.5$.

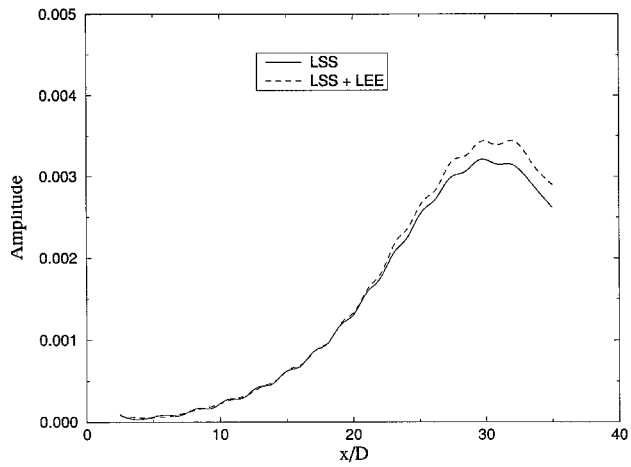

Fig. 6 Streamwise development of the amplitude of pressure fluctuations at $r/D = 12$.

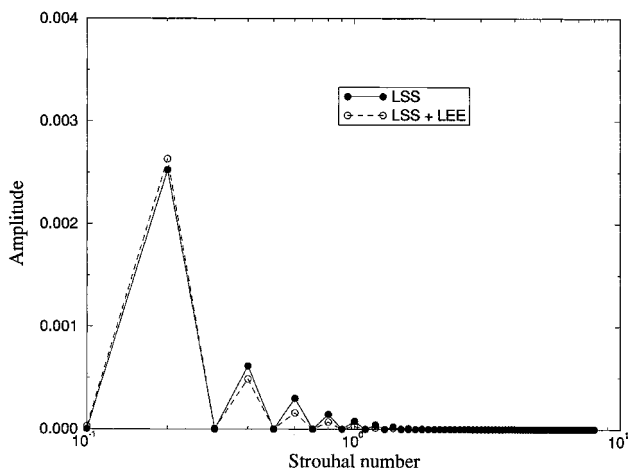

Fig. 7 Pressure spectra at $x/D = 25$, $r/D = 12$.

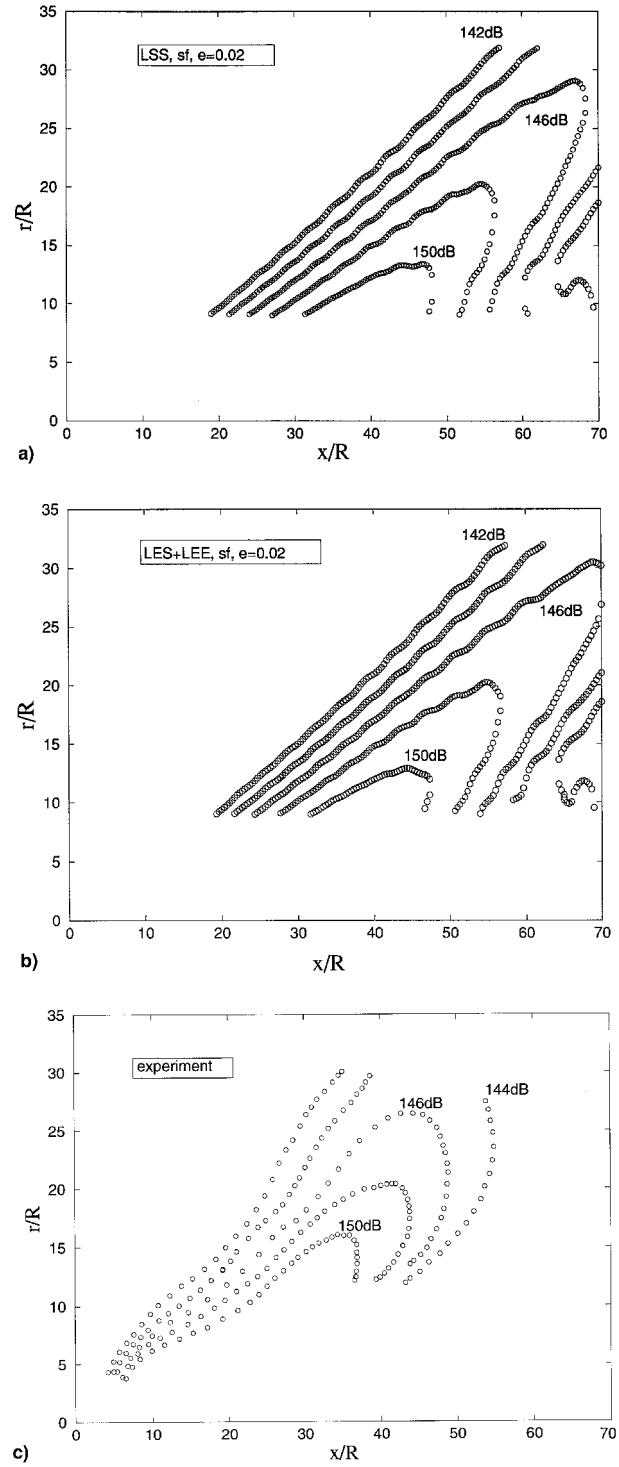

Fig. 8 Sound pressure level contours for a) large-scale calculations, b) large-scale and linearized Euler calculations, and c) the Troutt and McLaughlin experiment.[31]

experiment occurs at a larger angle than the computed results. This is attributed to the three-dimensional mechanisms.[31]

The solution sensitivity to matching boundary location, which was chosen at $r/D = 5$ and 7.5, respectively, is also investigated. Figure 10 shows the comparison of the axial distribution of rms values of pressure at $r/D = 7.5$ and 10. One can see that the solution is independent of the matching boundary location, which is denoted by RM in Fig. 10. However, if the matching boundary is placed in a region close to the jet flow where nonlinear effects cannot be neglected, errors could arise.

In the previous computations, the CPU times required on Cray Y-MP, at the NASA Lewis Research Center, are 24.05 and 31.14 h for the zonal approach and large-scale simulation,[10] respectively. Identical grid sizes are used in both computations. Further improvement can be achieved with the use of improved higher-order schemes with low dissipation/dispersion errors in both the inner nonlinear LES region and outer linearized Euler equations region.

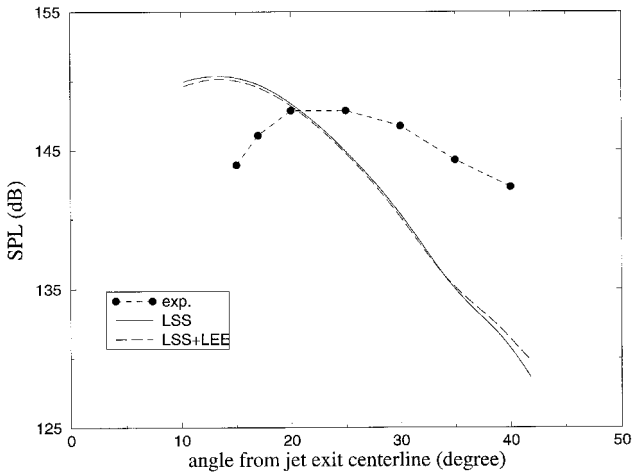

Fig. 9 Directivity of jet noise at $\bar{R}/D = 24$.

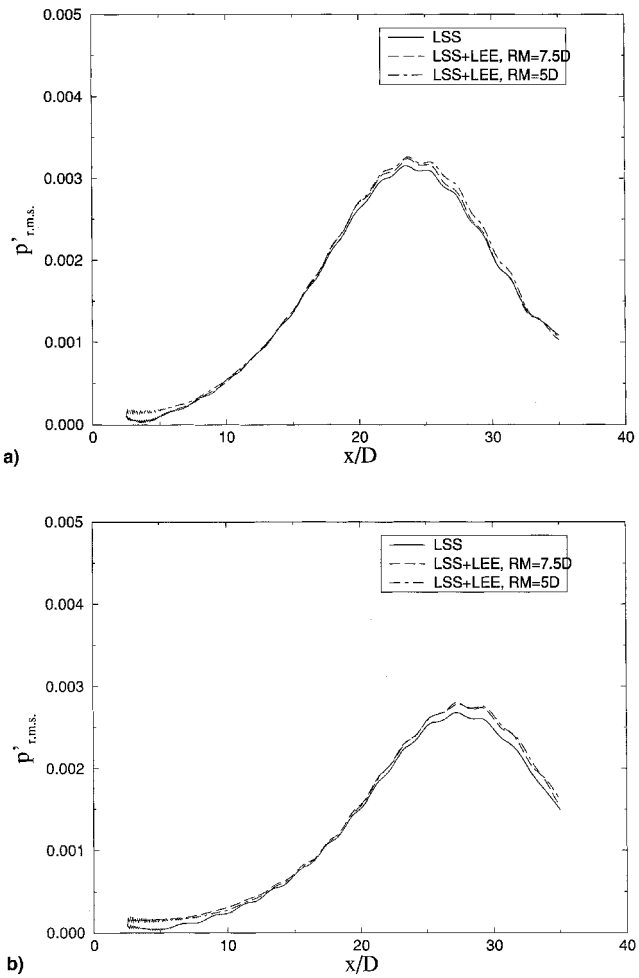

Fig. 10 Comparison of rms values of pressure at r/D = a) 7.5 and b) 10.

Conclusions

A zonal approach for direct computation of sound generation and propagation from a supersonic jet is investigated. The computational domain is split into a nonlinear acoustic source generation regime and a linear acoustic wave propagation regime. The unsteady flow in the nonlinear acoustic source region is governed by the large-scale equations, which are the filtered compressible Navier–Stokes equations. The linearized Euler equations are used to describe the sound wave propagation in the linear acoustic region. The computed results show that no spurious wave is generated in the matching region and the computational cost is reduced by 30% when compared with the direct simulation using large-scale equations alone. This reduction in computational cost becomes significant when the approach is extended to three-dimensional simulations.

References

[1]Seiner, J. M., McLaughlin, D. K., and Liu, C. H., "Supersonic Jet Noise Generated by Large-Scale Instabilities," NASA TP-2072, Sept. 1982.

[2]Zaman, K. B. M. Q., "Flow Field and Near and Far Sound Field of a Subsonic Jet," *Journal of Sound and Vibration*, Vol. 106, No. 1, 1986, pp. 1–6.

[3]Mankbadi, R. R., and Liu, J. T. C., "Sound Generated Aerodynamically Revisited: Large-Scale Structures in a Turbulent Jet as a Source of Sound," *Philosophical Transactions of the Royal Society of London, Series A: Mathematical and Physical Sciences*, Vol. 311, No. 183, 1984, pp. 183–217.

[4]Mankbadi, R. R., "The Self Noise from Ordered Structures in a Low Mach Number Jet," *Journal of Applied Mechanics*, Vol. 57, No. 1, 1990, pp. 241–246.

[5]Mankbadi, R. R., "Dynamics and Control of Coherent Structure in Turbulent Jets," *Applied Mechanics Reviews*, Vol. 45, No. 6, 1992, pp. 219–247.

[6]Tam, C. K. W., "Jet Noise Generated by Large-Scale Coherent Motion," *Aeroacoustics of Flight Vehicles: Theory and Practice. Vol. 1: Noise Source*, edited by H. H. Hubbard, NASA RP-1258, 1991, Chap. 6.

[7]Morris, P. J., Giridharan, M. G., and Lilley, G. M., "The Turbulent Mixing of Compressible Free Shear Layers," *Proceedings of the Royal Society of London*, Vol. 431, No. 1882, 1990, pp. 219–243.

[8]Tam, C. K. W., and Chen, P., "Turbulent Mixing Noise from Supersonic Jets," *AIAA Journal*, Vol. 32, No. 9, 1994, pp. 1774–1780.

[9]Mankbadi, R. R., Hayder, M. E., and Povinelli, L. A., "The Structure of Supersonic Jet Flow and Its Radiated Sound," *AIAA Journal*, Vol. 32, No. 5, 1994, pp. 897–906.

[10]Mankbadi, R. R., Shih, S. H., Hixon, R., and Povinelli, L. A., "Direct Computation of Sound Radiation by Jet Flow Using Large-Scale Equations," AIAA Paper 95-0680, Jan. 1995.

[11]Shih, S. H., Hixon, R., and Mankbadi, R. R.,"Three Dimensional Structure in a Supersonic Jet: Behavior near Centerline," AIAA Paper 95-0681, Jan. 1995.

[12]Hardin, J. C., and Pope, D. S., "Sound Generation by Flow over a Two-Dimensional Cavity," *AIAA Journal*, Vol. 33, No. 3, 1995, pp. 407–412.

[13]Hardin, J. C., and Pope, D. S., "High Reynolds Number Computational Aeroacoustics," *Proceedings of the 1st Joint CEAS/AIAA Aeroacoustics Conference*, Vol. 2, AIAA, Washington, DC, 1995, pp. 897–906.

[14]Viswanathan, K., and Sankar, L. N., "Toward the Direct Calculation of Noise: Fluid/Acoustic Coupled Simulation," *AIAA Journal*, Vol. 33, No. 12, 1995, pp. 2271–2279.

[15]Mankbadi, R. R., Hixon, R., Shih, S. H., and Povinelli, L. A., "On the Use of Linearized Euler Equations in the Prediction of Jet Noise," AIAA Paper 95-0505, Jan. 1995.

[16]Lyrintzis, A. S., and Mankbadi, R. R., "Prediction of the Far-Field Jet Noise Using Kirchhoff's Formulation," *AIAA Journal*, Vol. 34, No. 2, 1996, pp. 413–416.

[17]Freund, J. B., Lele, S. K., and Moin, P., "Matching of Near/Far-Field Equation Sets for Direct Computations of Aerodynamic Sound," AIAA Paper 93-4326, Oct. 1993.

[18]Erlebacher, G., Hussaini, M. Y., Speziale, C. G., and Zang, T. A., "Toward the Large-Eddy Simulation of Compressible Turbulent Flows," Inst. for Computer Applications in Science and Engineering, NASA Langley Research Center, Rept. 90-76, Hampton, VA, Oct. 1990.

[19]Smagorinsky, J., "General Circulation Experiments with the Primitive Equations, I. The Basic Experiment," *Monthly Weather Review*, Vol. 91, 1963, pp. 99–164.

[20]Edison, T. M., "Numerical Simulation of Turbulent Rayleigh-Bernard Problem Using Numerical Subgrid Modeling," *Journal of Fluid Mechanics*, Vol. 158, Sept. 1985, pp. 245–268.

[21]Hardin, J. C., "Recent Insights into Computational Aero-Acoustics," *Computational Aero- and Hydro-Acoustics*, edited by R. R. Mankbadi, A. S. Lyrintzis, O. Baysal, L. A. Povinelli, and M. Y. Hussaini, FED-Vol. 147, The American Society of Mechanical Engineers, New York, 1993, pp. 1–12.

[22]Gottlieb, D., and Turkel, E., "Dissipative Two-Four Methods for Time-Dependent Problems," *Mathematics of Computation*, Vol. 30, No. 136, 1976, pp. 703–723.

[23]Bayliss, A., and Maestrello, L., "Simulation of Instabilities and Sound Radiation in a Jet," *AIAA Journal*, Vol. 19, No. 7, 1981, pp. 835–841.

[24]Maestrello, L., Bayliss, A., and Turkel, E., "On the Interaction of a Sound Pulse with the Shear Layer of an Axisymmetric Jet," *Journal of Sound and Vibration*, Vol. 74, No. 2, 1981, pp. 281–301.

[25]Frendi, A., Maestrello, L., and Bayliss, A., "Coupling Between a Supersonic Boundary Layer and a Flexible Surface," *AIAA Journal*, Vol. 31, No. 4, 1993, pp. 708–713.

[26]Frendi, A., Maestrello, L., and Bayliss, A., "Coupling Between Plate Vibration and Acoustic Radiation," *Journal of Sound and Vibration*, Vol. 177, No. 2, 1994, pp. 207–226.

[27]Ragab, S. A., and Sheen, S., "The Nonlinear Development of Supersonic Instability Waves in a Mixing Layer," *Physics of Fluids A*, Vol. 3, No. 3, 1991, pp. 553–566.

[28]Farouk, B., Oran, E. S., and Kailasanath, K., "Numerical Simulations of the Structure of Supersonic Shear Layers," *Physics of Fluids A*, Vol. 3, No. 11, 1991, pp. 2786–2798.

[29]Hixon, R., Shih, S. H., and Mankbadi, R. R., "Evaluation of Boundary Conditions for Computational Aeroacoustics," *AIAA Journal*, Vol. 33, No. 11, 1995, pp. 2006–2012.

[30]Tam, C. K. W., and Burton, D. E., "Sound Generated by Instability Waves of Supersonic Flows, Part 2: Axisymmetric Jets," *Journal of Fluid Mechanics*, Vol. 138, Jan. 1984, pp. 273–295.

[31]Troutt, T. R., and McLaughlin, D. K., "Experiments on the Flow and Acoustic Properties of a Moderate Reynolds Number Supersonic Jet," *Journal of Fluid Mechanics*, Vol. 116, March 1982, pp. 123–156.

[32]Tam, C. K. W., and Webb, J. C., "Dispersion-Relation-Preserving Finite Difference Schemes for Computational Acoustics," *Journal of Computational Physics*, Vol. 107, No. 2, 1993, pp. 262–281.

[33]Bayliss, A., and Turkel, E., "Far Field Boundary Condition for Compressible Flows," *Journal of Computational Physics*, Vol. 48, No. 2, 1982, pp. 182–199.

[34]Enquist, B., and Majda, A., "Radiation Boundary Conditions for Acoustic and Elastic Wave Calculations," *Communications on Pure and Applied Mathematics*, Vol. 32, No. 3, 1979, pp. 313–357.

[35]Hagstrom, T., and Hariharan, S. I., "Far Field Expansion for Anisotropic Wave Equations," *Proceedings of the 2nd IMACS Symposium on Computational Acoustics*, edited by D. Lee, A. Cakmak, and R. Vichnevetsky, Vol. 2, North-Holland, 1990, pp. 283–294.